Available online at www.sciencedirect.com
SCIENCE DIRECT®
Physics of the Earth and Planetary Interiors 152 (2005) 67–77
PHYSICS OF THE EARTH AND PLANETARY INTERIORS
www.elsevier.com/locate/pepi

The axial ratio of hcp iron at the conditions of the Earth's inner core

C.M.S. Gannarelli[a], D. Alfè[a,b], M.J. Gillan[a,*]

[a] *Physics and Astronomy Department, University College London, Gower Street, London WC1E 6BT, UK*
[b] *Department of Earth Sciences, University College London, Gower Street, London WC1E 6BT, UK*

Received 26 September 2004; received in revised form 1 June 2005; accepted 3 June 2005

Abstract

We present ab initio calculations of the high-temperature axial *c*/*a* ratio of hexagonal-close-packed (hcp) iron at Earth's core pressures, in order to help interpret the observed seismic anisotropy of the inner core. The calculations are based on density functional theory, which is known to predict the properties of high-pressure iron with good accuracy. The temperature dependence of *c*/*a* is determined by minimising the Helmholtz free energy at fixed volume and temperature, with thermal contributions due to lattice vibrations calculated using harmonic theory. Anharmonic corrections to the harmonic predictions are estimated from calculations of the thermal average stress obtained from ab initio molecular dynamics simulations of hcp iron at the conditions of the inner core. We find a very gradual increase of axial ratio with temperature. This increase is much smaller than found in earlier calculations, but is in reasonable agreement with recent high-pressure, high-temperature diffraction measurements. This result casts doubt on an earlier interpretation of the seismic anisotropy of the inner core.

PACS: 62.20.D; 62.50.+p; 71.15.Ap; 91.35.−x

Keywords: Ab initio; Anisotropy; Core; Elasticity

1. Introduction

In the last few years, there have been a number of ab initio studies of iron at high temperatures and pressures, in an effort to understand the properties of the Earth's solid inner core (Stixrude et al., 1994, 1997; Stixrude and Cohen, 1995; Söderlind et al., 1996; Wasserman et al., 1996; Vočadlo et al., 1997, 2003; Vocadlo et al., 2000; Belonoshko et al., 2003; Laio et al., 2000; Alfè et al., 2001; Steinle-Neumann et al., 1999, 2001, 2002), including its elastic properties. A controversial issue, addressed by some of this work, concerns the elastic anisotropy of the inner core (Creager, 1992; Tromp, 1993), i.e. the fact that compressional waves are observed to traverse the core region some 3–4% faster along the Earth's rotational axis than in the equatorial plane. It is widely assumed that the phase of Fe in the

* Corresponding author. Tel.: +44 20 7679 7049; fax: +44 20 7679 1360.
E-mail address: m.gillan@ucl.ac.uk (M.J. Gillan).
URL: http://www.cmmp.ucl.ac.uk/∼mjg.

0031-9201/$ – see front matter © 2005 Elsevier B.V. All rights reserved.
doi:10.1016/j.pepi.2005.06.003

inner core is hexagonal-close-packed (hcp), and it has become clear that to understand the elastic properties it is necessary to know how the axial ratio c/a depends on temperature and pressure. In order to provide information about this, we present here ab initio calculations of the axial ratio of hcp iron over a range of pressures and temperatures relevant to the inner core.

Ab initio calculations on pure crystalline iron are very relevant for understanding the inner core, even though the core is known to contain light impurities (the leading candidates are O, Si and S), and is believed to contain Ni as well as Fe (Poirier, 1994). Recent estimates (Alfè et al., 2002a) suggest that the fraction of light impurities in the inner core is approximately 8.5 mol%, and this low fraction will probably not change its properties greatly. The Ni content will also probably make only a small difference, since the electronic structures of Ni and Fe are so similar. The determination of the properties of pure Fe is thus essential as a starting point for further refinements. The common assumption that Fe in the inner core is in the hcp structure has recently been challenged (Vočadlo et al., 2003; Belonoshko et al., 2003), and it is possible that the crystal structure is different in different parts of the core (Song and Helmberger, 1998; Ishii and Dziewonski, 2002; Beghein and Trampert, 2003). However, in order to make progress, it is clearly essential to understand the properties of the leading candidates, of which hcp is certainly one. It is well established that density functional theory (DFT) (Hohenberg and Kohn, 1964; Kohn and Sham, 1965; Jones and Gunnarsson, 1989) gives a rather accurate description of Fe and other transition metals, both under ambient conditions, and under high pressures and temperatures. This is known from comparisons with experiment for a wide range of properties, including the equilibrium lattice parameter under ambient conditions, elastic constants, magnetic properties, phonon frequencies (Stixrude et al., 1994; Söderlind et al., 1996; Vočadlo et al., 1997; Vocadlo et al., 2000); the pressure–volume relationship at high pressures, the phonon density of states and the Hugoniot (Wasserman et al., 1996; Mao et al., 2001; Alfè et al., 2001).

A number of groups have used DFT calculations to investigate the elastic constants of hcp Fe under inner-core conditions. The early calculations were performed at zero temperature (Stixrude and Cohen, 1995; Steinle-Neumann et al., 1999), and led to the suggestion that elastic anisotropy could be explained by a preferential alignment of crystalline c-axes with the Earth's rotational axis. However, more recent work has indicated a strong temperature dependence of the elastic constants (Steinle-Neumann et al., 2001, 2002), including a crossing of the c_{11} and c_{33} constants at approximately 1500 K, which would result in a reversal of the necessary crystalline alignment. It appears that the strong temperature dependence of the elastic constants is due in part to a rapid increase of the axial ratio with increasing temperature. However, this work can be questioned, because it is based upon a statistical mechanical approximation known as the particle-in-cell (PIC) model (Hirshfelder et al., 1954; Holt and Ross, 1970; Holt et al., 1970; Ree and Holt, 1973; Westra and Cowley, 1975; Cowley et al., 1990), which may not be reliable. In addition, independent PIC calculations have failed to reproduce their results (Gannarelli et al., 2003). Very recently, experimental work (Ma et al., 2004) has shown that this strong c/a variation with temperature is not observed at pressures up to 160 GPa. Our aim in this paper is to perform calculations of the high temperature axial ratio, which are, as far as possible, free of statistical mechanical approximations.

The calculation of phonon dispersion relations using DFT is nowadays completely routine, and this makes it possible to obtain the Helmholtz free energy F of a high-temperature crystal without any statistical mechanical approximations, provided that anharmonicity can be ignored. Phonon dispersion relations for Fe in both the magnetic body-centred cubic and the hcp structures have been reported by several groups (Vocadlo et al., 2000). The equilibrium value of c/a can then be obtained for given V and T by minimising F with respect to c/a. Of course, at temperatures near the melting point, it is not obvious that anharmonic corrections to F can be neglected. However, direct DFT molecular dynamics simulations allow the calculation of the thermal average stress tensor (Oganov et al., 2001), so that the equilibrium c/a can be found by requiring that the stress tensor be isotropic; such direct simulations completely include anharmonicity. The DFT calculation of phonon frequencies is straightforward and relatively inexpensive, but ab initio molecular dynamics demands much larger computational resources. Our strategy in this work is therefore to base most of the calculations on the harmonic approximation, but to use a small number

of molecular dynamics simulations to estimate anharmonic corrections to the equilibrium c/a.

The rest of this paper is organised as follows: in Section 2 we present the technical background to our electronic structure calculations, and describe the statistical mechanical principles of our harmonic and molecular-dynamics calculations. In Section 3 we describe our harmonic calculations, including the technical tests we performed to ensure their accuracy. In Section 4 we present our ab initio molecular-dynamics results. Discussion of our results for the temperature and pressure dependence of the axial ratio follows in Section 5.

2. Techniques

The principal quantity in this work is the ab initio Helmholtz free energy $F(V, q, T)$ as a function of the volume V, axial ratio $q = c/a$ and temperature T. The temperature in the Earth's core is far above the Debye temperature of Fe, so most of the present work is based on the standard expression of classical statistical mechanics for the free energy:

$$F(V,q,T) = -k_{\mathrm{B}}T \ln \left\{ \frac{1}{\Lambda^{3N}} \int \mathrm{d}\mathbf{r}_1 \ldots \mathrm{d}\mathbf{r}_N \times \exp\left[\frac{-U_{\mathrm{AI}}(\mathbf{r}_1 \ldots \mathbf{r}_N; T_{\mathrm{el}})}{k_{\mathrm{B}}T} \right] \right\} \quad (1)$$

where T is the temperature and Λ the thermal wavelength. Comments will be made later about quantum effects for the nuclear degrees of freedom, when we refer to results at temperatures below the Debye temperature. The quantity $U_{\mathrm{AI}}(\mathbf{r}_1 \ldots \mathbf{r}_N; T_{\mathrm{el}})$ is the ab initio Helmholtz free energy of the system when the atoms are fixed at the positions $\{\mathbf{r}_i\}$; U_{AI} is a free energy because it includes thermal excitation of the electrons, at electronic temperature T_{el}, as described by finite temperature density functional theory (Mermin, 1965). Since we are interested in the case of full thermal equilibrium, we have $T_{\mathrm{el}} = T$. In the present work, the DFT calculation of U_{AI} is made using the exchange-correlation energy given by the PW91 generalised gradient approximation (Wang and Perdew, 1991). The implementation of DFT is the projector augmented wave (PAW) scheme (Blöchl, 1994; Kresse and Joubert, 1999) with core radii, augmentation charge radii, etc., as reported in (Alfè et al., 2000). As in our previous work, atomic states up to and including 3p are treated as core states, but the high-pressure response of 3s and 3p states is included via an empirical pair potential. This approximation is tested using spot-checks with 3p electrons included in the valance set. All calculations were performed using the VASP code (Kresse and Furthmüller, 1996a,b).

In practice, the ab initio Helmholtz free energy is separated into perfect lattice, harmonic and anharmonic contributions:

$$F = F_{\mathrm{perf}} + F_{\mathrm{harm}} + F_{\mathrm{anharm}}. \quad (2)$$

Here $F_{\mathrm{perf}} = U_{\mathrm{AI}}(\mathbf{R}_1 \ldots \mathbf{R}_N; T_{\mathrm{el}})$ is the ab initio free energy with all atoms fixed on their perfect-lattice positions $\{\mathbf{R}_i\}$. The harmonic contribution F_{harm} is given by (Alfè et al., 2001)

$$F_{\mathrm{harm}} = 3k_{\mathrm{B}}T \ln \frac{\hbar\bar{\omega}}{k_{\mathrm{B}}T}, \quad (3)$$

with $\bar{\omega}$ the geometric mean phonon frequency:

$$\ln \bar{\omega} = \frac{1}{N_{\mathbf{k}s}} \sum_{\mathbf{k}s} \ln \omega_{\mathbf{k}s}, \quad (4)$$

where $N_{\mathbf{k}s}$ is the total number of k-points and phonon-branches, the sum being taken over the first Brillouin zone. $\bar{\omega}$ is a function of V, q and T_{el}. As usual, the phonon frequencies $\omega_{\mathbf{k}s}$ at each wavevector $\mathbf{k}$ are obtained by diagonalising the dynamical matrix, whose elements are defined in terms of the force-constant matrix $\Phi_{ls\alpha,l't\beta}$ as:

$$D_{s\alpha,t\beta}(\mathbf{k}) = \frac{1}{M} \sum_{l'} \Phi_{ls\alpha,l't\beta} \exp[\mathrm{i}\mathbf{k} \cdot (\mathbf{R}^0_{l't} - \mathbf{R}^0_{ls})], \quad (5)$$

where M is the mass of each atom. Here $\mathbf{R}^0_{ls}$ is the equilibrium position of the sth atom in the lth primitive cell. Calculation of the force-constant matrix Φ is performed by the small-displacement method (Kresse et al., 1995; Alfè et al., 2001; Alfé, 1998), in which each atom in the primitive cell is given a small displacement, and DFT is used to calculate the resulting force on every atom in a large repeating cell. The calculation of the dynamical matrix and hence the mean frequency $\bar{\omega}$ must be taken to convergence with respect to the size of the repeating cell. For the hcp structure, the entire Φ matrix is calculated by performing only

two independent displacements, as explained in Alfè et al. (2001). Within the harmonic approximation, the equilibrium c/a at given atomic volume and temperature is determined by calculating $F_{\mathrm{perf}}(q)$ and $F_{\mathrm{harm}}(q)$ at a series of q values, and by minimising the quantity $F_{\mathrm{perf}}(q) + F_{\mathrm{harm}}(q)$ numerically.

Our estimates of anharmonic corrections to the equilibrium c/a are based on ab initio molecular dynamics simulations. These are performed in the canonical ensemble, using an Andersen thermostat (Andersen, 1980). The determination of the equilibrium c/a is based on a calculation of the time-averaged stress tensor $\sigma_{\alpha\beta}$. The system is in hydrostatic equilibrium with respect to variation of q when $\sigma_{33} - \sigma_{11} = 0$. In comparing with harmonic predictions, it is useful to note that the components of the thermal average stress tensor are related to the ab initio harmonic free energy by

$$\langle \sigma_{\alpha\beta} \rangle = \frac{1}{V_0} \lim_{\varepsilon_{\alpha\beta} \to 0} \left(\frac{\partial F}{\partial \varepsilon_{\alpha\beta}} \right)_T , \tag{6}$$

where $\varepsilon_{\alpha\beta}$ is the infinitesimal strain tensor and V_0 is the volume of the system before application of the strain. In particular, for our constant volume calculations of $F(V, q, T)$, we can write

$$\langle \sigma_{33} - \sigma_{11} \rangle = \frac{3q}{2V} \left(\frac{\partial F}{\partial q} \right)_{V,T} . \tag{7}$$

This means that the stress component $\langle \sigma_{33} - \sigma_{11} \rangle$ within the harmonic approximation can be obtained by taking the derivative with respect to q of the free energy $F_{\mathrm{perf}}(q) + F_{\mathrm{harm}}(q)$.

3. Harmonic calculation of the equilibrium axial ratio

In order to determine the equilibrium axial ratio in harmonic theory, the two quantities that it is necessary to calculate are the perfect lattice free energy F_{perf}, and the geometric mean phonon frequency $\bar{\omega}$, both as function of volume, axial ratio c/a and electronic temperature. The calculation of these quantities is presented in the following subsections, and the results for the equilibrium axial ratio are presented in Section 3.3. The precision we need to achieve in the calculations is set by the precision with which we wish to determine the equilibrium axial ratio. As a guideline, we set ourselves the target of obtaining c/a to a precision of ± 0.005.

3.1. Perfect lattice free energy

DFT results for the perfect lattice free energy for $c/a = 1.6$ were reported earlier by Alfè et al. (2001), and were more recently reported by Gannarelli et al. (2003) for q in the range 1.48–1.72. The present calculations are closely related to the previous ones, but we have introduced some refinements. We have calculated F_{perf} for electronic temperatures in the range 1000–7000 K. For T_{el} in this range, we find that an $8 \times 8 \times 5$ Monkhorst–Pack k-point sampling set provides a precision of better than 1.5 meV atom^{-1}. The plane-wave cutoff has been set to achieve complete continuity in the curve $F_{\mathrm{perf}}(q)$, and to ensure that at every point on this curve, the calculated energy and stress components are converged to within our required targets.

For the set of T_{el} mentioned above, we have calculated F_{perf} for c/a in the range 1.54–1.70, at steps of 0.01 and for volumes between 6.8 and 8.8 Å^3 at steps of 0.2 Å^3, as well as at three particular volumes of interest, 6.97, 7.50 and 8.67 Å^3. A parameterisation essentially exactly fitting the data consists of a cubic polynomial in c/a, whose coefficients are fitted to quartic polynomials in T_{el}. As a point of reference for our later discussion, we have used these results to calculate the equilibrium axial ratio at $T = 0$ as a function of volume. We have converted the results to obtain q as a function of pressure by using the $P(V)$ relation from Stixrude et al. (1994). In Fig. 1, we compare the resulting values of $q(P)$ with very recent room-temperature synchrotron measurements (Ma et al., 2004) in the pressure range 60–160 GPa. In both cases, we see a very slight increase of q with pressure, though the theoretical values are lower by about 0.008. The theoretical results shown in Fig. 1 do not include quantum mechanical lattice effects due to zero-point energy. This will be addressed in Section 3.3.

3.2. Harmonic calculations

As explained in Section 2, the harmonic vibrational free energy is determined entirely by $\bar{\omega}$. Values of $\bar{\omega}$ must be converged with respect to k-point sampling, cell size and atomic displacement, and we must ensure

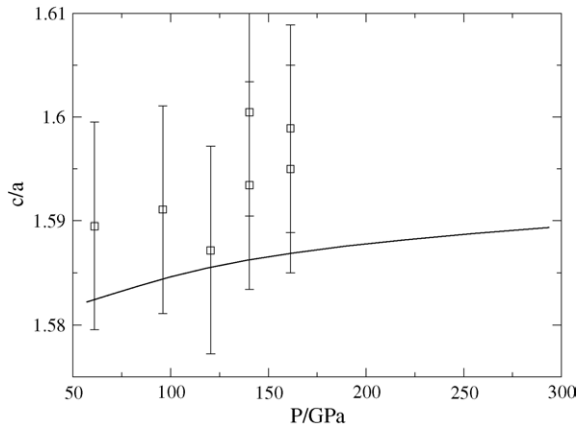

Fig. 1. Calculated equilibrium axial ratio of hcp Fe at zero temperature as a function of pressure (solid curve), compared with diffraction results of Ma et al. (2004) (open squares with error bars).

that this convergence is achieved across the required range of c/a. In order to achieve the required tolerance in the harmonic free energy, systematic errors in $\bar{\omega}$ must not vary with respect to q by more than 0.1%.

We have designed a strategy for ensuring convergence of $\bar{\omega}$. In our initial tests, we adopt a displacement of 0.01 Å, which has been used in previous calculations (Alfè et al., 2001). With this displacement, we determine the k-point sampling needed to obtain convergence for a 16-atom supercell. We then study convergence with respect to cell size, the k-point sampling for each cell size being chosen in the light of the k-point sampling tests of the 16-atom system. This set of tests tells us the cell size needed. To conclude the tests, we then address convergence of atomic displacement and k-point sampling for this cell size. All these tests are performed at $T_{\mathrm{el}} = 1000$ K. This temperature is deliberately chosen to be much lower than the temperatures of real interest. We do this because the fineness of k-point sampling needed to achieve a given degree of convergence decreases with increasing temperature. One can therefore be sure that if convergence is achieved with respect to k-point sampling at 1000 K, it will certainly be achieved at higher temperatures.

For the 16-atom system, $\bar{\omega}$ was calculated for Monkhorst–Pack sets up to $9 \times 9 \times 6$. We find that for a Monkhorst–Pack $5 \times 5 \times 3$ grid, $\bar{\omega}$ is converged to within 0.01%. Next, a set of supercells was chosen, such that the dimension along the hexagonal axis is similar to the dimension in the basal plane. Sizes chosen were 16 ($2 \times 2 \times 2$), 36 ($3 \times 3 \times 2$), 54 ($3 \times 3 \times 3$), 96 ($4 \times 4 \times 3$), 128 ($4 \times 4 \times 4$) and 150 ($5 \times 5 \times 4$) atoms. For each cell size, we calculate $\bar{\omega}$ using k-point sampling that is equivalently finer than the converged value of $5 \times 5 \times 3$ in the 16-atom system. We find that for a 54-atom system, $\bar{\omega}$ is converged to within 0.5%, however the consistency between calculations for different values of c/a at this cell size, is much better than our tolerance. Finally, k-point and displacement convergence were carried out on the 54-atom system. We found that for a $3 \times 3 \times 2$ Monkhorst–Pack grid and a displacement of 0.01 Å, $\bar{\omega}$ is converged to within approximately 1% in absolute terms, but, again, to well within our tolerances for non-cancelling errors. These tests were all performed for both $c/a = 1.60$ and 1.70. All the harmonic results that follow were based upon values of $\bar{\omega}$ calculated for these values of supercell size, k-point sampling and displacement.

Calculations of $\bar{\omega}$ were performed for atomic volumes of 6.97, 7.50 and 8.97 Å^3, for c/a from 1.58 to 1.70 in steps of approximately 0.03, and for electronic temperatures of 2000, 4000 and 6000 K. We parameterised $\ln \bar{\omega}(q)$ for each volume and temperature using a second order polynomial in q, which gave an effectively exact fit to the results.

3.3. Harmonic results for equilibrium axial ratio

Equilibrium values of c/a were obtained at 6.97, 7.50 and 8.67 Å^3 and temperatures of 0, 2000, 4000 and 6000 K, by analytic minimisation of the total harmonic free energy $F_{\mathrm{perf}}(q) + F_{\mathrm{harm}}(q)$, using the polynomial parameterisations described above for $\ln \bar{\omega}(V, q, T_{\mathrm{el}})$ and $F_{\mathrm{perf}}(V, q, T_{\mathrm{el}})$. Results are shown in Fig. 2, together with the previous theoretical results of Steinle-Neumann et al. (2001) and the very recent experimental results of Ma et al. (2004). Note that all the theoretical results show the variation of c/a with T at fixed volume, whereas the experimental results are at the fixed pressure of 161 GPa. The present results differ greatly from the earlier theoretical results, in that we find only a very moderate increase of c/a with temperature. The experimental increase of c/a with temperature is also far smaller than the predictions of Steinle-Neumann et al. (2001), and is, if anything, smaller than the variation that we predict. More detailed discussion will be given in Section 5.

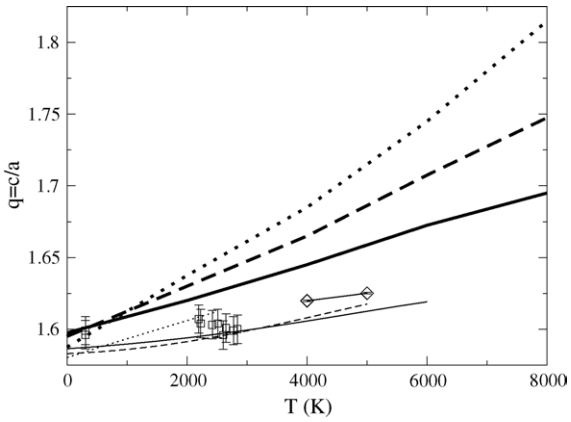

Fig. 2. Calculated equilibrium axial ratio as a function of temperature for different volumes. For this work (light curves) atomic volumes are 6.97 Å^3 (solid curve), 7.50 Å^3 (dashed curve) and 8.67 Å^3 (dotted curve). For Steinle-Neumann et al. (2001) (heavy curves) volumes are 6.81 Å^3 (solid curve), 7.11 Å^3 (dashed curve) and 7.41 Å^3 (dotted curve). Also shown are diffraction measurements due to Ma et al. (2004) at 7.73 Å^3/atom (open squares with error bars) and our own ab initio MD calculations (open diamonds) at 6.97 Å^3.

We now return to the question of quantum corrections to the energy of lattice vibrations. At zero temperature, there exists a 'zero point' contribution to the energy per atom

$$E_Z = \frac{1}{2N_{\mathbf{k}s}} \sum_{\mathbf{k}s} \hbar\omega_{\mathbf{k}s}. \tag{8}$$

Using our calculated phonon frequencies, we have computed this energy as a function of q at an atomic volume $V = 6.97$ Å^3. By differentiating with respect to q, we obtain a contribution to the stress $\sigma_{33} - \sigma_{11}$, varying at $V = 6.97$ Å^3 between -230 MPa at $q = 1.58$ and -910 MPa at $q = 1.70$. This would shift the equilibrium axial ratio by no more than 0.001. It is expected that this contribution will become even smaller as temperature increases.

4. Molecular dynamics calculations

The determination of the equilibrium axial ratio by ab initio molecular dynamics is based on the calculation of stresses; specifically on the stress difference $\sigma_{33} - \sigma_{11}$, which disappears for the equilibrium value of c/a. In order to apply this technique successfully, a number of technical sources of error must be brought under control. Firstly, the duration of the run must be long enough to reduce statistical errors to within an acceptable level; secondly, the size of the simulation cell must be large enough; and thirdly, electronic k-point sampling must be adequate. The first two of the convergence questions can be addressed in detail using classical molecular dynamics simulations, and we have performed tests of this kind as described below. The question of k-point convergence will be discussed when we present our ab initio molecular dynamics calculations in Section 4.2.

Although ab initio molecular dynamics calculations fully include anharmonicity, they are very demanding in terms of computational resources, so that we can only perform these calculations at a very small number of state points. Our aim is to put limits on the possible size of anharmonic corrections to the stress, and hence to c/a. Our ab initio molecular dynamics results for $\sigma_{33} - \sigma_{11}$ can be compared with our harmonic calculations by using Eq. (7) to calculate $\sigma_{33} - \sigma_{11}$ in the harmonic approximation. Since anharmonicity is negligible at low temperatures, the harmonic and molecular dynamics calculations of the stress should be in close agreement under these conditions. This provides a further check both on our harmonic and molecular dynamics results.

4.1. Molecular dynamics simulations for an embedded-atom model

Our tests on statistical and system-size errors were performed using an embedded atom model (EAM) for Fe, similar to that used by Belonoshko et al. (2000). In the EAM, the total energy E_{tot} of a system of N atoms is represented as the sum of two contributions. First, an empirical, repulsive pair potential, and secondly, a sum of embedding energies for each atom, representing quantum mechanical band-structure effects:

$$E_{\text{tot}} = E_{\text{pair}} + E_{\text{embed}},$$
$$E_{\text{pair}} = \frac{1}{2}\sum_{i\neq j} \phi(|\mathbf{r}_i - \mathbf{r}_j|), \qquad E_{\text{embed}} = \sum_i f(\rho_i),$$
$$\rho_i = \sum_{j(\neq i)} \psi(|\mathbf{r}_i - \mathbf{r}_j|) \tag{9}$$

where $\phi(r)$ and $\psi(r)$ have the inverse power forms

$$\phi(r) = \epsilon \left(\frac{a}{r}\right)^n \quad \text{and} \quad \psi(r) = \left(\frac{a}{r}\right)^m, \tag{10}$$

and $f(\rho_i) = -\epsilon C(\rho_i)^{\frac{1}{2}}$. In practice, both ϕ and ψ are cut off smoothly by making the transformation

$$\phi(r) \to \phi_{\mathrm{SF}}(r) = \begin{cases} \phi(r) + \beta + \gamma r & r < r_0 \\ \alpha(r_1 - r)^3 & r_0 < r < r_1 \\ 0 & r_1 < r \end{cases}, \tag{11}$$

where r_0 and r_1 are cutoff radii, with α, β and γ chosen such that ϕ, ϕ' and ϕ'' are continuous at r_0. The form guarantees that these three functions are also continuous at r_1. In the present calculations, we use $r_1 = 7$ Å, $r_0 = 0.9r_1$. The parameters have been modified somewhat from those given by Belonoshko et al. (2000), in order to reproduce better our ab initio molecular dynamics simulations on solid and liquid Fe (Alfè et al., 2001, 2002b). The parameters we user are: $n = 5.93$, $m = 4.788$, $\epsilon = 0.1662$ eV, $a = 3.4714$ Å and $C = 16.55$.

In order to assess the length of run needed to reduce the statistical error on $\sigma_{33} - \sigma_{11}$ to an acceptable level, we have performed molecular dynamics runs at several system sizes and at a number of different thermodynamic state points. An illustration of such a run is given in Fig. 3. On the basis of these calculations we find that, in order to reduce the r.m.s. statistical errors

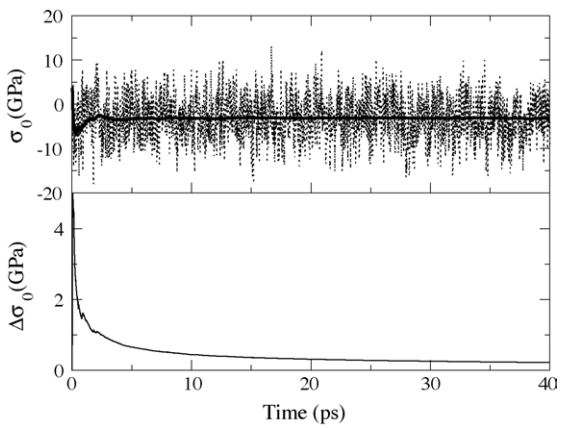

Fig. 3. Instantaneous (dotted curve) and average (solid) value of $\sigma_0 = \sigma_{33} - \sigma_{11}$ (upper plot) and standard error (lower plot) for a 40 ps run for $V = 6.97$ Å^3/atom, $T = 4000$ K and $c/a = 1.65$ in the embedded atom model.

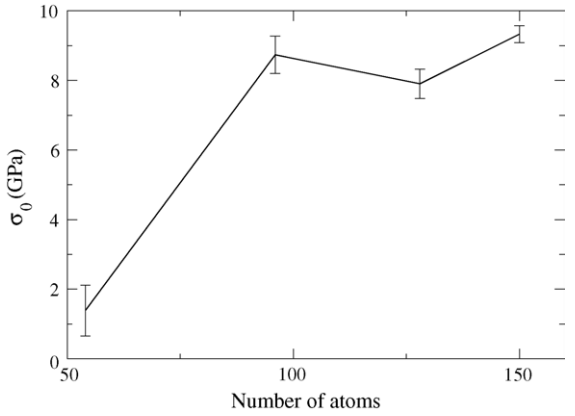

Fig. 4. Fifteen picoseconds time-averaged calculations of $\sigma_0 = \sigma_{33} - \sigma_{11}$ for a variety of cell sizes within the embedded atom model.

to within 1 GPa, for example, we require a run of length 3–4 ps. Since the r.m.s. error is inversely proportional to the square root of the length of run, we may immediately infer the length of run necessary to obtain any required precision. From statistical mechanics, we expect that for a given length of run, the r.m.s. error on the stress components will decrease with increasing system size as $N^{-\frac{1}{2}}$, where N is the number of atoms. We find that this is consistent with tests performed on system size, with r.m.s. errors on a 1.5 ps average falling from 2 GPa for a 54-atom cell, to 1 GPa for 150 atoms. To test size errors we performed runs on systems containing 54, 96, 128 and 150 atoms at identical state points. Fig. 4 shows the effect of system size on $\sigma_{33} - \sigma_{11}$. Error bars show r.m.s. statistical errors as described above. We see that for a system of 96 atoms, the error due to size effects is within approximately 0.6 GPa.

It follows from these tests that in order to calculate $\sigma_{33} - \sigma_{11}$ to a tolerance needed to determine the equilibrium axial ratio to within 0.005, it should be enough to perform ab initio molecular dynamics simulations of 1 ps on 96 atoms.

As a further test of our techniques, we have compared molecular dynamics results for $\sigma_{33} - \sigma_{11}$ with the predictions of harmonic theory for the embedded atom model. Fig. 5 presents the molecular dynamics and harmonic results for $V = 6.97$ Å^3, $c/a = 1.65$ for a range of temperatures. Because of the gradual variation of $\sigma_{33} - \sigma_{11}$ with temperature, we use longer runs of up to 5 ps. Cell sizes are converged within the limits discussed above. We see that at low temperatures,

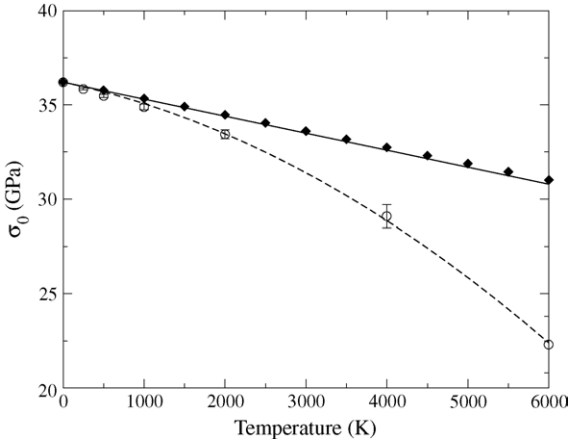

Fig. 5. Molecular dynamics (open circles) and harmonic (diamonds) calculations of $\sigma_0 = \sigma_{33} - \sigma_{11}$ for a 6.97 Å^3 cell in the embedded atom model, with $c/a = 1.70$. The dashed curve represents a second-order fit to the MD data, while the solid line is its tangent at 0 K. In agreement with thermodynamic theory, this coincides the harmonic calculations of the stress.

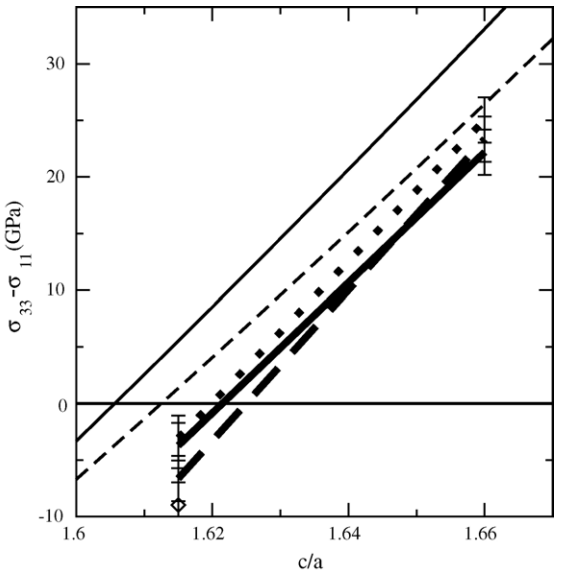

Fig. 6. Comparison of ab initio MD (heavy curves) and harmonic (light) results for the stress $\sigma_{33} - \sigma_{11}$. Solid lines are at 4000 K, dashed lines at 5000 K. The dotted line shows results for 150-atom molecular dynamics at 4000 K. The diamond represents a 96-atom run including 3p states explicitly in the valence set. All calculations were performed for an atomic volume of 6.97 Å^3. For comparison with earlier PIC calculations due to Steinle-Neumann et al. (2001), see Fig. 2.

the molecular dynamics results reproduce well the predictions of harmonic theory. This agreement provides additional confirmation that the statistical and system-size errors on the molecular dynamics calculations are very small. The deviation, rising to around 8.5 GPa at 6000 K, shows the high-temperature emergence of anharmonic effects.

4.2. Ab initio molecular dynamics results

We have performed ab initio molecular dynamics simulations at an atomic volume of 6.97 Å^3, in which we have calculated $\sigma_{33} - \sigma_{11}$. The molecular dynamics calculations are performed using exactly the same DFT methods as in the harmonic calculations. From the tests on the embedded atom model, we already have a good indication of the cell size and length of run necessary, but the question of k-points must also be addressed. To do this, we calculate $\sigma_{33} - \sigma_{11}$ for several disordered configurations, selected from classical MD trajectories, both with Γ-point sampling and with larger numbers of k-points. Our tests are performed for a 96-atom system, with an atomic volume of 6.97 Å^3 and an axial ratio of 1.65. The molecular dynamics simulation from which the configurations were drawn was performed at 5000 K. We took four snapshots at intervals of 0.2 ps. For this state point, $\sigma_{33} - \sigma_{11}$, with Γ-point sampling is equal to 7.0 ± 2 GPa. For a $2 \times 2 \times 2$ k-point grid, it is equal to 7.1 ± 2.6 GPa. Similar tests were performed to ensure that size effects were consistent with the embedded atom model.

Our ab initio calculations at 6.97 Å^3 were performed for $c/a = 1.615$ and 1.66, and for $T = 4000$ K and 5000 K. Fig. 6 shows results for $\sigma_{33} - \sigma_{11}$ along with harmonic predictions. We see that our molecular dynamics results closely resemble the predictions of harmonic theory, and vary in the same way with c/a. However, even allowing for the error bars, there is an appreciable difference between the harmonic and MD results. One of the technical sources of error which could account for this discrepancy is system size effects. In order to check this, we have repeated the 5000 K runs using 150 atoms instead of 96. The results of this test suggest that system-size errors could account for most of this discrepancy. We have also examined other technical sources of error, such as plane-wave cutoff and k-point sampling; however, as described above, there are not capable of producing

such a discrepancy. It is possible in principle that some of this discrepancy can be attributed to anharmonic effects, but it is difficult to separate this from other effects with any certainty. Even allowing for the remaining uncertainties, it seems certain that anharmonic effects are not capable of shifting the equilibrium axial ratio by more than about 0.01.

We have also used ab initio MD to test another significant question. All our harmonic and MD calculations up to this point have treated 3p and 3s electrons as core states, but with the high-pressure response of these states treated via an empirical pair potential. In order to test the effect of this approximation, we have repeated the 96-atom MD calculations at 5000 K with 3p electrons explicitly included in the valence set. The resulting stress $\sigma_{33} - \sigma_{11}$ agrees with our other results within our error bars. This indicates that the effects of this approximation are negligible for our present purposes.

5. Conclusions

We have shown that it is rather straightforward to calculate harmonic free energies, and hence calculate the variation of c/a within the harmonic approximation. Because these calculations are computationally inexpensive, it is possible to apply them to a wide variety of thermodynamic state points. Since our earlier comparisons with experiment (Mao et al., 2001) show the reliability of our density functional methods for calculating the phonon frequencies for iron at high pressures, we expect our predictions of the temperature dependence of c/a to be reliable. We have also shown that direct ab initio molecular dynamics simulation can be used to put limits on the possible size of anharmonic effects. These methods are rather expensive, but provide a means to perform "spot checks" on our results. The molecular dynamics calculations show that anharmonic corrections to the c/a ratio are small, even at temperatures near the melting point.

The main scientific conclusion from the work is that c/a varies only rather weakly with temperature, and that its variation becomes weaker as pressures approach those of the inner core. Quantitatively, at a pressure of 100 GPa, c/a increases from 1.585 at zero temperature, to 1.61 at the melting point, and at 300 GPa, from 1.59 at zero temperature, to 1.62 at the melting point. These results do not support the earlier predictions by Steinle-Neumann et al. (2001) of a strong increase of c/a with temperature within the particle-in-cell approximation. Interestingly, the results we have found are very similar to our own predictions from the particle-in-cell approximation (Gannarelli et al., 2003). This implies that this approximation cannot be responsible for the large discrepancy between the present results and those of Steinle-Neumann et al. (2001). This finding of a rather weak increase of c/a with temperature is strongly supported by the recent diffraction experiments of Ma et al. (2004). Even allowing for the significant error bars on their c/a results, it seems clear that at 161 GPa, 2000 K, c/a is no bigger than about 1.61 at most. Our results would indicate a value of around 1.60 under these conditions.

Our results have implications for understanding the elastic anisotropy of the inner core. Steinle-Neumann et al. (2001) predicted a reversal of the crystalline alignment required to explain the anisotropy of the inner core, due to a crossing of the c_{11} and c_{33} elastic moduli at approximately 1500 K. They attribute this to the strong temperature-dependence they find in c/a. Since our results cast doubt on this strong temperature dependence, they also cast doubt on the proposed explanation for the elastic anisotropy. However, in order to resolve this question fully, we need to make ab initio predictions of the elastic moduli, that are free of statistical mechanical approximations. The methods we have presented here should be capable of achieving this, and we hope to be able to present such results in due course.

Acknowledgments

The work of CMSG is supported by a NERC studentship, and the work of DA by a Royal Society fellowship and by an award from the Leverhulme Trust. The calculations were performed using UCL facilities, supported by a JREI grant and by SRIF funding. The authors thank G.D. Price and L. Vočadlo for useful discussions.

References

Alfé, D., 1998. Program available at http://chianti.geol.ucl.ac.uk/ dario.

Alfè, D., Gillan, M.J., Price, G.D., 2002. Ab initio chemical potentials of solid and liquid solutions and the chemistry of the Earth's core. J. Chem. Phys. 116, 7127.

Alfè, D., Kresse, G., Gillan, M.J., 2000. Structure and dynamics of liquid iron under Earth's core conditions. Phys. Rev. B 61, 132.

Alfè, D., Price, G.D., Gillan, M.J., 2001. Thermodynamics of hexagonal-close-packed iron under Earth's core conditions. Phys. Rev. B 64, 045123.

Alfè, D., Price, G.D., Gillan, M.J., 2002. Iron under Earth's core conditions: liquid-state thermodynamics and high-pressure melting curve from ab initio calculations. Phys. Rev. B 65, 165118.

Andersen, H.C., 1980. Molecular dynamics simulations at constant pressure and/or temperature. J. Chem. Phys. 72, 2384.

Beghein, C., Trampert, J., 2003. Robust normal mode constraints on inner-core anisotropy from model space search. Science 299, 552.

Belonoshko, A.B., Ahuja, R., Johansson, B., 2000. Quasi-ab initio molecular dynamic study of Fe melting. Phys. Rev. Lett. 84, 3638.

Belonoshko, A.B., Ahuja, R., Johansson, B., 2003. Stability of the body-centred-cubic phase of iron in the Earth's inner core. Nature 424, 1032.

Blöchl, P.E., 1994. Projector augmented-wave method. Phys. Rev. B 50, 953.

Cowley, E.R., Gross, J., Gong, Z.X., Horton, G.K., 1990. Cell-cluster and self-consistent calculations for a model sodium-chloride crystal. Phys. Rev. B 42, 3135.

Creager, K.C., 1992. Anisotropy of the inner core from differential travel-times of the phases pkp and pkikp. Nature 356, 309.

Gannarelli, C.M.S., Alfè, D., Gillan, M.J., 2003. The particle-in-cell model for ab initio thermodynamics: implications for the elastic anisotropy of the Earth's inner core. Phys. Earth Planet In. 139, 243.

Hirshfelder, J.O., Curtiss, C.F., Bird, R.B., 1954. Molecular Theory of Gases and Liquids. John Wiley and Sons, Inc., New York.

Hohenberg, P., Kohn, W., 1964. Inhomogeneous electron gas. Phys. Rev. 136, B864.

Holt, A.C., Hoover, W.G., Gray, S.G., Shortle, D.R., 1970. Comparison of the lattice-dynamics and cell-model approximations with Monte-Carlo thermodynamic properties. Physica 49, 61.

Holt, A.C., Ross, M., 1970. Calculations of the Grüneisen parameter of some models of the solid. Phys. Rev. B 1, 2700.

Ishii, M., Dziewonski, A.M., 2002. The innermost inner core of the Earth: evidence for a change in anisotropic behaviour at the radius of about 300 km. Proc. Natl. Acad. Sci. U.S.A. 99, 14026.

Jones, R.O., Gunnarsson, O., 1989. The density functional formalism, its applications and prospects. Rev. Mod. Phys. 61, 689.

Kohn, W., Sham, L., 1965. Self-consistent equations including exchange and correlation effects. Phys. Rev. 140, A1133.

Kresse, G., Furthmüller, J., 1996. Efficiency of ab initio total energy calculations for metals and semiconductors using a plane-wave basis set. Comput. Mater. Sci. 6, 15.

Kresse, G., Furthmüller, J., 1996. Efficient iterative schemes for ab initio total-energy calculations using a plane-wave basis set. Phys. Rev. B 54, 11169.

Kresse, G., Furthmüller, J., Hafner, J., 1995. Force constant approach to phonon dispersion relations of diamond and graphite. Europhys. Lett. 32, 729.

Kresse, G., Joubert, D., 1999. From ultrasoft pseudopotentials to the projector augmented-wave method. Phys. Rev. B 59, 1758.

Laio, A., Bernard, S., Chiarotti, G.L., Scandolo, S., Tosatti, E., 2000. Physics of iron at Earth's core conditions. Science 287, 1027.

Ma, Y., Somayazulu, M., Shen, G., Mao, H.K., Shu, J., Hemley, R., 2004. In situ X-ray diffraction studies of iron to Earth-core conditions. Phys. Earth Planet In. 143–144, 455.

Mao, H.K., Xu, J., Struzhkin, V.V., Shu, J., Hemley, R.J., Sturhahn, W., Hu, M.Y., Alp, E.E., Vočadlo, L., Alfè, D., Price, G.D., Gillan, M.J., Schwoerer-Böhning, M., Häusermann, D., Eng, P., Shen, G., Giefers, H., Lübbers, R., Wortmann, G., 2001. Phonon density of states of iron up to 153 GPa. Science 292, 914.

Mermin, N.D., 1965. Thermal properties of the inhomogeneous electron gas. Phys. Rev. 137, A1441.

Oganov, A.R., Brodholt, J.P., Price, G.D., 2001. The elastic constants of $MgSiO_3$ perovskite at pressures and temperatures of the Earth's mantle. Nature 411, 934.

Poirier, J.P., 1994. Light elements in the Earth's outer core: a critical review. Phys. Earth Planet In. 85, 319.

Ree, F.H., Holt, A.C., 1973. Thermodynamic properties of the alkali-halide crystals. Phys. Rev. B 8, 826.

Söderlind, P., Moriarty, J.A., Willis, J.M., 1996. First-principles theory of iron up to earth-core pressures: structural, vibrational, and elastic properties. Phys. Rev. B 53, 14063.

Song, X.D., Helmberger, D.V., 1998. Seismic evidence for an inner core transition zone. Science 282, 924.

Steinle-Neumann, G., Stixrude, L., Cohen, R.E., 1999. First-principles elastic constants for the hcp transition metals Fe, Co, and Re at high pressure. Phys. Rev. B 60, 791.

Steinle-Neumann, G., Stixrude, L., Cohen, R.E., 2002. Physical properties of iron in the inner core. In: Dehant, V., Creager, K., Zatman, S., Karato, S.-I. (Eds.), Core Structure, Dynamics and Rotation. American Geophysical Union, Washington, DC 137–161.

Steinle-Neumann, G., Stixrude, L., Cohen, R.E., Gülseren, O., 2001. Elasticity of iron at the temperature of the Earth's inner core. Nature 413, 57.

Stixrude, L., Cohen, R.E., 1995. High-pressure elasticity of iron and anisotropy of Earth's inner-core. Science 267, 1972.

Stixrude, L., Cohen, R.E., Singh, D.J., 1994. Iron at high pressure: linearized-augmented-plane-wave computations in the generalized-gradient approximation. Phys. Rev. B 50, 6442.

Stixrude, L., Wasserman, E., Cohen, R.E., 1997. Composition and temperature of Earth's inner core. J. Geophys. Res. [Space Phys.] 102, 24729.

Tromp, J., 1993. Support for anisotropy of the Earth's inner-core from free oscillations. Nature 366, 678.

Vočadlo, L., Alfè, D., Gillan, M.J., Wood, I.G., Brodholt, J.P., Price, G.D., 2003. Possible thermal and chemical stabilisation of body-centred-cubic iron in the Earth's core. Nature 424, 536.

Vocadlo, L., Brodholt, J., Alfe, D., Gillan, M.J., Price, G.D., 2000. Ab initio free energy calculations on the polymorphs of iron at core conditions. Phys. Earth Planet In. 117, 123.

Vočadlo, L., de Wijs, G.A., Kresse, G., Gillan, M.J., Price, G.D., 1997. First principles calculations on crystalline and liquid iron at Earth's core conditions. Faraday Discuss. 106, 205.

Wang, Y., Perdew, J.P., 1991. Correlation hole of the spin-polarized electron gas, with exact small-wave-vector and high-density scaling. Phys. Rev. B 44, 13298.

Wasserman, E., Stixrude, L., Cohen, R.E., 1996. Thermal properties of iron at high pressures and temperatures. Phys. Rev. B 53, 8296.

Westra, K., Cowley, E.R., 1975. Cell-cluster expansion for an anharmonic solid. Phys. Rev. B 11, 4008.